AIAA JOURNAL
Vol. 49, No. 12, December 2011

Enhancement of a Flapping Wing Using Path and Dynamic Topology Optimization

Jung-Sun Choi* and Liangyu Zhao†
Hanyang University, Seoul 133-791, Republic of Korea
Gyung-Jin Park‡
Hanyang University, Ansan City 426-791, Republic of Korea
Sunil K. Agrawal§
University of Delaware, Newark, Delaware 19716
and
Raymond M. Kolonay¶
U.S. Air Force Research Laboratory, Wright-Patterson Air Force Base, Ohio 45433, USA

DOI: 10.2514/1.J050834

The flapping wing of a micro air vehicle is optimized to enhance performance while some rigidity is kept with a specific mass. A work flow for the design of the flapping wing is defined. The performances to be enhanced are thrust coefficient and propulsive efficiency. The flapping kinematics of the flapping wing is determined by solving a path optimization problem that maximizes the performances. The optimization process is carried out based on a well-defined surrogate model. The surrogate model is made from the results of two-dimensional fluid dynamic analysis. The kriging method is employed to establish the surrogate model and a genetic algorithm is used for the multi-objective function problem. Dynamic topology optimization is performed to find the distribution of reinforcement. Certain rigidity can be kept by the results of topology optimization. A dynamic topology optimization method is developed by modification of the equivalent static loads method for nonlinear static response structural optimization. Three-dimensional computational fluid dynamic analysis is performed based on the optimum values of the path optimization to evaluate the external loads for the topology optimization process. The process of the defined work flow is materialized by interfacing various software systems.

Nomenclature

AR	=	aspect ratio
a	=	dimensionless length from the leading edge to the pivot point
$\mathbf{b}$	=	design variable vector
b_i	=	design variable in the ith element
$\mathbf{b}^{(k)}$	=	design variable vector at the cycle number k
$b_i^{(k)}$	=	design variable at the cycle number k in the ith element
$\mathbf{b}^{(k+1)}$	=	design variable vector at the cycle number $k+1$
$b_i^{(k+1)}$	=	design variable at the cycle number $k+1$ in the ith element
$\mathbf{b}^{(0)}$	=	initial design variable vector
$b_{\min}$	=	lower bound of the design variable
$\mathbf{C}(\mathbf{b})$	=	viscous damping matrix
C_D	=	drag coefficient
$\bar{C}_D$	=	time-averaged drag coefficient
C_L	=	lift coefficient
$\bar{C}_L$	=	time-averaged lift coefficient
C_M	=	pitch moment coefficient
C_T	=	thrust coefficient
$\bar{C}_T$	=	time-averaged thrust coefficient
c	=	chord, m
E	=	Young's modulus, Gpa
E_i	=	Young's modulus of the ith element
E_0	=	initial Young's modulus
F_x	=	x component of the resulting aerodynamics force acting on the airfoil, N
F_y	=	y component of the resulting aerodynamics force acting on the airfoil, N
f	=	frequency, Hz
$\mathbf{f}$	=	static load vector
$\mathbf{f}(t)$	=	dynamic load vector
$\mathbf{f}_{\text{eq}}(s)$	=	equivalent static loads vector
$\mathbf{f}_{\text{eq}}^{(k)}(s)$	=	equivalent static loads vector at the cycle number k
$\mathbf{f}^T\mathbf{z}$	=	compliance
h	=	reduced plunging amplitude with respect to the chord
$\mathbf{K}(\mathbf{b})$	=	stiffness matrix
k	=	reduced frequency
Ma	=	Mach number
$\mathbf{M}(\mathbf{b})$	=	mass matrix
Re	=	Reynolds number
S	=	reference area
St	=	Strouhal number
T	=	period, s
u	=	far-field flow velocity, m/s
V	=	total volume of the structure
$\mathbf{v}_e$	=	volume of each element
$\mathbf{z}(s)$	=	static displacement vector
$\mathbf{z}(t)$	=	dynamic displacement vector
ε_1	=	specified value of density
ε_2	=	percent of the total design variable
ε_3	=	density value of design update
η	=	propulsive efficiency
θ	=	angle between the chord and the far-field flow speed direction

Received 5 August 2010; revision received 22 March 2011; accepted for publication 1 July 2011.

*Graduate Student, Department of Mechanical Engineering.
†Postdoctoral Fellow, Department of Mechanical Engineering. Member AIAA.
‡Professor, Department of Mechanical Engineering; gjpark@hanyang.ac.kr. Senior Member AIAA (Corresponding Author).
§Professor, Department of Mechanical Engineering.
¶Aerospace Engineer, Air Vehicles Directorate. Member AIAA.

ρ = density of fluid around the airfoil, kg/m^3
ρ_m = density of the material, kg/m^3
ϕ = phase angle of pitching motion leading plunging motion
ω = angular frequency, rad/s

I. Introduction

THE flapping-wing micro air vehicle (FWMAV), inspired by birds, bats, insects, fishes and whales, has been receiving more and more attention from military and civilian application domains since the micro air vehicle (MAV) was generally defined by the Defense Advanced Research Projects Agency in 1997 [1]. Some unique advantages of FWMAVs, such as high maneuverability and hovering capability, make the research in this area quite active. Early studies, such as the Garrick theory [2], focused on simplified models. As research has evolved, more practical and sophisticated models have been employed. The continuous development of computational methods makes it possible to simulate a real insect flying in the air [3], and some FWMAVs were fabricated during the past years. For example, Jones and Platzer [4] proposed an unconventional biplane flapping-wing MAV in 2006. In this model, the thrust is generated by the biplane pair of the two trailing flapping wings and the lift is generated by the front stationary wing, as illustrated in Fig. 1. The present work is closely related to this design.

Recent experimental and computational achievements showed that the flapping performance, such as the thrust coefficient and the propulsive efficiency, depends on the flapping kinematics significantly. Thus, from the design perspective, the flapping path should be determined such that it maximizes the performance of an FWMAV. Anderson et al. [5] showed that oscillating foil could have a very high propulsive efficiency, as high as 87%, under specific combinations of the flapping kinematics by water-tunnel experiments. Pesavento and Wang [6] found that the optimized flapping-wing motions could save up to 27% of the aerodynamic power required by the optimal steady flight. In 2005, Tuncer and Kaya [7] employed the steepest ascent search algorithm to maximize a linear combination of the maximum thrust and the propulsive efficiency for flapping airfoils. In 2007, Kaya and Tuncer [8] performed optimization with a NURBS (nonuniform rational B-splines) flapping path instead of a sinusoidal flapping path in their previous paper, and a gradient-based search algorithm was employed to find the optimum. In 2009, Kaya et al. [9] extended their optimization scheme to a biplane configuration. Meanwhile, Soueid et al. [10] optimized the motion of a flapping airfoil using sensitivity functions. In Soueid et al.'s work, the objective function was a combination of several related parameters, such as the time-averaged thrust coefficient, the average power input and the average angle of attack.

In this research, path optimization is performed based on the paradigm of previous researchers [7]; however, different optimization methods are used to reduce the effort for path optimization. Path optimization based on a well-defined surrogate model using the kriging method is performed [11]. The surrogate model is established by using two-dimensional computational fluid dynamics (2-D CFD) analysis, because 3-D CFD analysis in the optimization process is prohibitively expensive. Obviously, 2-D CFD analysis cannot predict three-dimensional effects (e.g., the wing tip vortices and the spanwise flows). There are the differences between 2-D and the 3-D CFD analyses in terms of accuracy. However, we expect that the results of 2-D path optimization are an acceptable approximation for the 3-D CFD analysis. In path optimization, a multi-objective function and genetic algorithm are used [12]. The genetic algorithm can find a global solution while a gradient-based optimization can find a local optimum. After that, the optimum value of the path optimization is used for dynamic topology optimization.

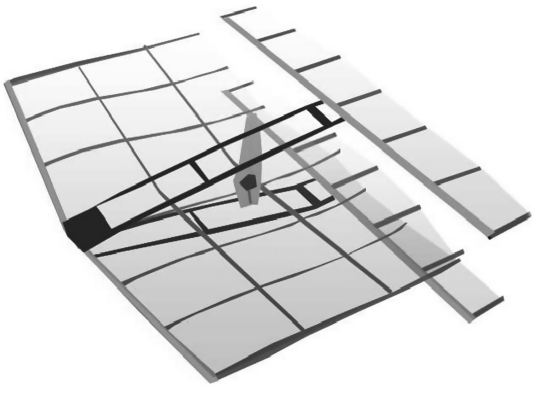

Fig. 1 Flapping-wing MAV model.

The flapping wing should pursue minimum mass and some rigidity to enhance the aerodynamic characteristics. In other words, the flapping-wing structure should have some flexibility and certain rigidity [13,14], and a small amount of rigidity guarantees flexibility. It is not yet known how rigid the flapping wing should be. Topology optimization finds the stiffest structure with a given mass. Therefore, topology optimization can propose rigidity with minimum mass. Topology optimization is carried out to keep a certain rigidity of the flapping wing with a specific mass. It is noted that there are not many studies on the structural design of the flapping wing. Some researchers have conducted topology optimization on the fixed wing of a MAV [15].

In this research a topology optimization method is newly developed for the flapping wing. Topology optimization determines the distribution of the reinforcement on the flapping wing. The distribution of the reinforcement can be regarded as the vein distribution of the wing, which mimics the wing of an insect. The pressure from the CFD analysis is imposed on the flapping wing as the external loads in the topology optimization process. It is noted that the pressures are imposed in the time domain. Generally, topology optimization is performed in a static sense. A dynamic topology optimization method is developed based on modification of a method called the equivalent static loads method for nonlinear static response structural optimization (ESLSO) [16–18].

The problem is solved by interfacing various software systems. The commercial computational fluid dynamics (CFD) system FLUENT [19] is used for unsteady aerodynamics analysis. Nastran [20] is used for dynamic analysis, and GENESIS [21] is used for topology optimization. The optimization process uses the genetic algorithm in MATLAB [22]. An in-house C++ program [23] is coded to link the systems. The research results are summarized and the future direction for the design of the flapping wing is proposed.

II. Flow of the Design Methodology

This work starts from a well-defined flapping wing, as illustrated in Fig. 1. The biplane pair of the trailing wings is flapping and generates the thrust force. The overall research flow is defined in Fig. 2. At first, path optimization is carried out to determine the motion of the flapping wing. The motion consists of the plunging motion and the pitching motion. In the optimization, the parameters for the path are the plunging amplitude, the pitching amplitude, and the phase angle between the two motions, and these parameters are used as design variables. The objective function to be maximized is a multi-objective function that is composed of the thrust coefficient and the propulsive efficiency and CFD analysis is required to evaluate the objective function. A gradient-based optimization process needs sensitivity information with respect to design variables, and it is well known that sensitivity analysis with CFD analysis is extremely expensive [10]. Therefore, a surrogate model is used in this research, and the kriging method is employed to establish the surrogate model [11]. Because 3-D analysis is highly costly, 2-D unsteady CFD analysis is conducted for the establishment of the surrogate model.

Responses such as the thrust coefficient and the propulsive efficiency are evaluated at various design points and the design points (samples) are defined by an orthogonal array. A genetic algorithm is selected to solve the multi-objective function problem defined from the surrogate model made by the kriging method [12]. The genetic algorithm may not be practical if we directly use CFD analysis,

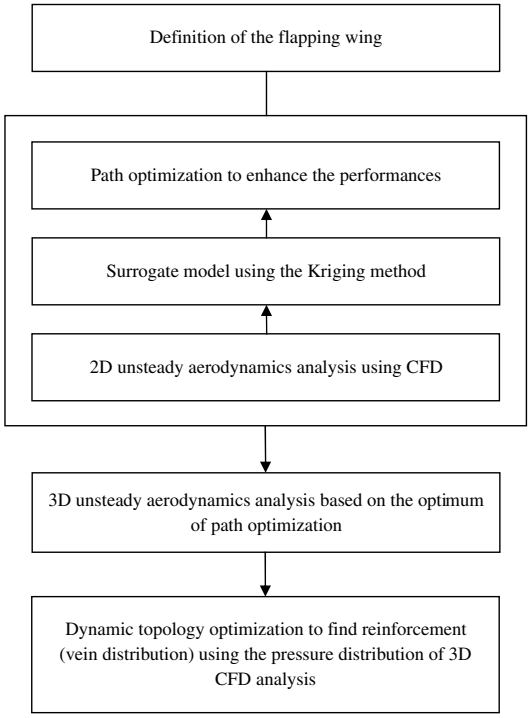

Fig. 2 Flow of the research.

because the algorithm requires many function calculations. Since the surrogate model is used, the function calculation in the optimization process is almost negligible.

For structural design, the pressures on the flapping wing are required, because they should be used as external loads on the structure. Only 3-D CFD analysis can provide the pressure distribution around the flapping wing. A computational model in three dimensions is made and 3-D unsteady CFD analysis is performed with the optimum values from the path optimization. The flapping motion is dynamic (transient) and we need the pressure distribution in the time domain. The 3-D unsteady CFD analysis results provide the pressure distribution in the time domain and this dynamic pressure distribution is used as the external loads for dynamic analysis of the flapping-wing structure.

As mentioned earlier, topology optimization is performed to have some rigidity with a given mass. The reinforcement in the flapping wing is determined in the topology optimization process. Topology optimization is generally carried out with static loads [24]. However, the flapping wing operates in the dynamic (transient) environment and the current topology optimization methods can be hardly used for the design of the flapping wing. A new topology optimization method is developed to handle the dynamic pressure distribution in the time domain by using ESLSO [25]. ESLSO has been extensively used for size and shape optimizations and it is modified for topology optimization in this research.

The logic for the current work may not be perfect because of the cost and the limitation of the technical problems. For example, if optimization with 3-D aeroelasticity analysis is used, the path and the structure can be optimized simultaneously. However, this approach does not seem to be realistic at this moment. Moreover, the pair of flapping wings should be considered together. The future direction of this research is proposed in a later section.

III. Path Optimization

This section starts with a description of the flapping motion. The involved governing equations and a well validated mesh for simulating the unsteady flowfield around an airfoil are also described. After the path optimization problem is defined, the surrogate model for the kriging method is constructed. Then, the optimum flapping kinematic parameters are obtained by a genetic algorithm. At the end of this section, 3-D CFD analysis is performed under these optimum parameters for a wing with a given aspect ratio. Meanwhile, the derivatives between flapping performances of the 2-D airfoil and ones of the 3-D wing are demonstrated.

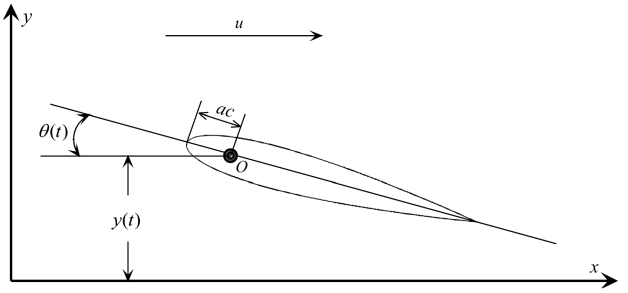

Fig. 3 Illustration of the flapping model.

A. Flapping-Wing System

The flapping motion, including the plunging and pitching motions, can be described as follows:

$$y(t) = hc\cos(\omega t) \tag{1}$$

$$\theta(t) = \theta_0\cos(\omega t + \phi) \tag{2}$$

where $y(t)$ stands for the plunging motion, $\theta(t)$ is the pitching motion, c is the chord length, h is the dimensionless plunging amplitude, ω is the angular frequency in rad/s, θ_0 is the pitching amplitude, and ϕ is the phase-shift angle of the pitching motion leading the plunging motion. The reduced frequency k is defined as

$$k = 2\pi fc/u = \omega c/u \tag{3}$$

where f is the flapping frequency in hertz and u is the flow velocity of the far field. This flapping model is illustrated using a 2-D airfoil in Fig. 3, where O is the pivot point and a is the dimensionless length from the leading edge to the pivot point with respect to the chord.

The Reynolds number Re and the Strouhal number St are

$$Re = \rho uc/\mu \tag{4}$$

$$St = fA/u \tag{5}$$

where ρ is the fluid density, μ is the fluid dynamic viscosity, and A is the wake width and can be estimated using the peak-to-peak excursion of the trailing edge or, more simply, by twice the plunging amplitude.

In classical aerodynamics, the lift coefficient C_L, the drag coefficient C_D, and the pitch moment coefficient C_M can be defined as

$$C_D = \frac{F_x}{0.5\rho u^2 S} \tag{6}$$

$$C_L = \frac{F_y}{0.5\rho u^2 S} \tag{7}$$

$$C_M = \frac{M_z}{0.5\rho u^2 SL} \tag{8}$$

where F_x and F_y are the components of the resulting aerodynamics force along horizontal (parallel with u direction) and vertical (normal to u direction) directions, respectively, S is the reference area and equals to c in value for a 2-D problem, M_z is the pitch moment with respect to the pivot point, and L is the reference length and equals to c here. The time-averaged thrust coefficient $\bar{C}_T$ and the power input coefficient $\bar{C}_P$ in one flapping cycle can be calculated by Eqs. (9) and (10). Correspondingly, the propulsive efficiency is defined in Eq. (11):

$$\bar{C}_T = -\bar{C}_D = -\frac{1}{T}\int_t^{t+T} C_D(t)\,\mathrm{d}t \tag{9}$$

$$\bar{C}_P = \frac{1}{T}\left(\int_t^{t+T} C_L(t)\dot{y}(t)\,\mathrm{d}t + \int_t^{t+T} C_M(t)\dot{\theta}(t)c\,\mathrm{d}t\right) \tag{10}$$

$$\eta = \bar{C}_T u/\bar{C}_P \tag{11}$$

where T is the period in seconds, with $T = 1/f$, and $\dot{y}(t)$ and $\dot{\theta}(t)$ are the first-order time derivation of $y(t)$ and $\theta(t)$, respectively. For simplicity, we also use C_D to stand for $\bar{C}_D$ and we use C_T for $\bar{C}_T$ in the next sections.

B. Two-Dimensional CFD Analysis

The commercial CFD solver FLUENT [17] is employed to simulate the unsteady flowfields around the moving wings with predefined motions. The time-dependent Navier–Stokes equations are solved using the finite volume method, assuming the incompressible laminar flow. The mass and momentum equations are solved in a fixed inertial reference frame incorporating a dynamic mesh. The continuity and the momentum equations are given as

$$\nabla \cdot \boldsymbol{V} = 0 \tag{12}$$

$$\rho\left(\frac{\partial \boldsymbol{V}}{\partial t} + \boldsymbol{V}\cdot\nabla\boldsymbol{V}\right) = -\nabla p + \mu\nabla^2\boldsymbol{V} \tag{13}$$

where $\boldsymbol{V}$ and p are velocity and pressure, respectively.

The hybrid mesh that is shown schematically in Fig. 4 is employed to compute the flowfield. The computational domain is divided into two distinct zones: moving zone and remeshing zone. The moving zone consists of the C-type structured quadrilateral mesh, and the remeshing zone consists of the unstructured triangular mesh. The airfoil is located in the center of the computational domain, and the no-slip wall boundary condition is applied. The spatial scale of each zone and corresponding boundary condition are also shown in Fig. 4. The whole moving zone mesh, including the interfaces between these two zones, moves with the airfoil together according to the predefined airfoil motion. In other words, the structured mesh near the airfoil always moves with the airfoil. This means remeshing only occurs at a distance of 20 to 45 reference lengths away from the airfoil body, which ensures that the flow simulation around the airfoil is somewhat affected by the moving mesh. The C-type mesh structure in the very close neighborhood of the airfoil is shown in Fig. 5. Figure 6 shows the results of the grid sensitivity analysis using six different kinds of mesh. The results are almost similar for the time histories of C_D. In Fig. 6, 201×101 and $0.0002c$ mean that the grid size is 201×101 nodes (201 along every single airfoil surface and 101 in the vertical direction) with the thickness of the first-layer grid around the airfoil equal to $0.0002c$. The hybrid mesh is generated by GAMBIT [26].

To validate the accuracy of the present approach, simulations are performed in seven periods with 500 and 1000 time steps in one plunging period under the conditions of $k = 2.0$, $h = 0.4$, $u = 34.7$ m/s ($Ma = 0.1$), $c = 0.064$ m, and $Re = 1.0 \times 10^4$. The coupling between the pressure and the velocity is achieved by means of the SIMPLEC algorithm. Meanwhile, the discretizations of pressure and momentum terms are the second-order scheme and the second-order upwind scheme. The time discretization is the first-order implicit scheme, which is a more straightforward method in

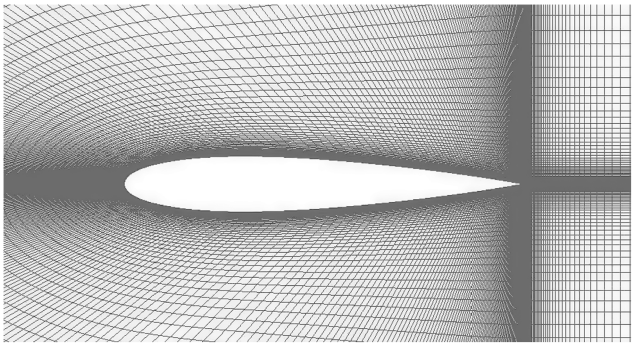

Fig. 5 C-type grid very close to the airfoil.

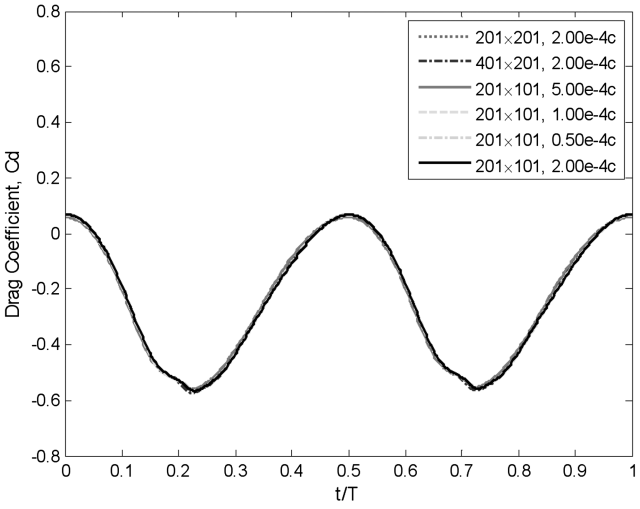

Fig. 6 Drag coefficients on six grid types.

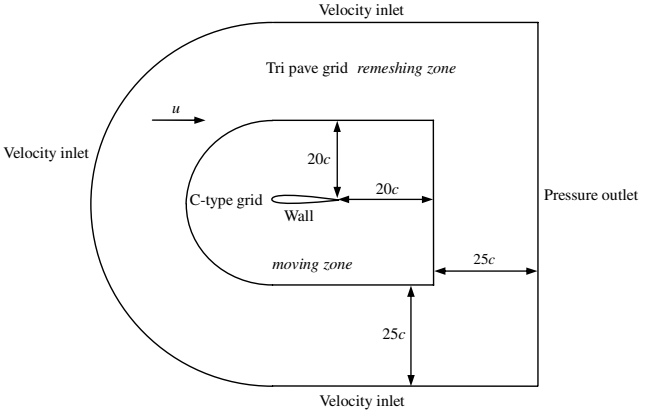

Fig. 4 Hybrid mesh topology with boundary conditions.

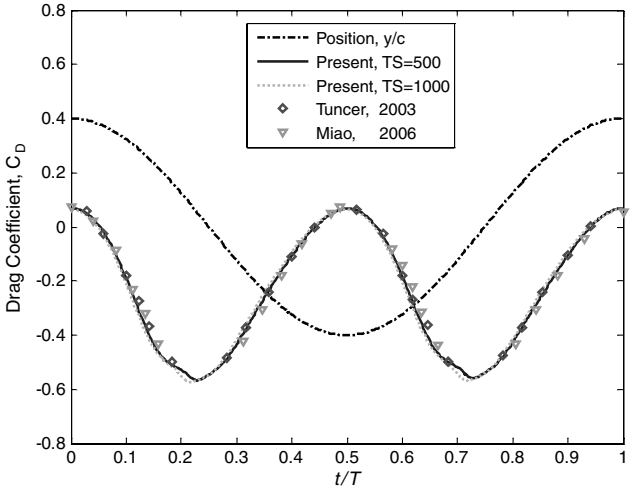

Fig. 7 Validation for the plunging motion.

FLUENT for the dynamic mesh module [27]. The time variation of the plunging position and the time histories of C_D in one period are illustrated in Fig. 7, and they are compared with the results obtained by Miao and Ho [13] and Tuncer and Kaya [28]. These four results show good agreement, although different mesh schemes are employed in these studies. Figure 7 also shows that the difference between 500 time steps and 1000 time steps is trivial; therefore, 500 time steps are good enough in this analysis. Based on the validation, 201×101 size grid with the first-layer thickness of $0.0002c$ and 500 time steps are employed for all of the simulations in the next sections.

C. Optimization Formulation

In the above section of the numerical method validation, the flight conditions match with those of [13,28]. In path optimization, the flight conditions are defined for a practical FWMAV, because the above flight conditions of $k = 2$, $u = 34.7$ m/s, flapping frequency is 172.6 Hz, $c = 0.064$ m, and $Re = 1.0 \times 10^4$ are unrealistic. Newly defined flight conditions are $k = 1$, $u = 3.0$ m/s, flapping frequency is 9.55 Hz, $c = 0.05$ m, and $Re = 1.0 \times 10^4$ for the path optimization. The path optimization problem for an NACA0012 airfoil [7] is formulated as follows:

Find

$$h, \theta_0, \phi$$

Minimize

$$f(h, \theta_0, \phi) = (1 - \beta)\frac{C_T - C_{T,\max}}{C_{T,\min} - C_{T,\max}} + \beta\frac{\eta - \eta_{\max}}{\eta_{\min} - \eta_{\max}} \qquad (14)$$

Subject to

$$0.8 \leqslant h \leqslant 2.5, 10.0 \leqslant \theta_0 \leqslant 30.0, 80.0 \leqslant \phi \leqslant 135.0$$

where β is the weight factor, $C_{T,\min}$ and $C_{T,\max}$ are the minimum and the maximum time-averaged thrust coefficients in the design array for constructing the kriging model, and $\eta_{\min}$ and $\eta_{\max}$ are the minimum and the maximum propulsive efficiency in the design array when constructing the kriging model. This objective function is equivalent to maximizing the time-averaged thrust coefficient and the propulsive efficiency simultaneously under the given weight factors.

D. Surrogate Model with the Kriging Method

In this research, the kriging model is employed as the approximation method, and the orthogonal array is employed as the design of experiments technique. The kriging method initiated from the geostatistical field can be considered as a member of the family of linear least-squares estimation algorithms [11]. The kriging model combines a global polynomial model plus a localized departure. This is why the kriging model is expected to find a good global approximation at an unobserved location for a nonlinear problem [11,12]. Based on the design space described, h is divided into seven levels, θ_0 has five levels, and ϕ has six levels, as shown in Table 1. The design array in this paper consists of the union of the 49 samples obtained using a classical orthogonal array and the eight vertices, which means 55 samples total. The high-fidelity results are obtained using FLUENT under the given flight conditions.

To make the surrogate model more flexible, two kriging models are constructed to fit the time-averaged thrust coefficient and propulsive efficiency, respectively. Two kriging models have the same design variables, which are the dimensionless plunging amplitude, the pitching amplitude, and the phase angle. Five design points not belonging to the samples are selected to evaluate these two surrogate models, as shown in Table 2. The largest relative error between the high-fidelity model and the surrogate model is 5.3%, and these two kriging models are supposed to be good enough to predict the time-averaged thrust coefficient and the propulsive efficiency.

Table 1 Design space, factors, and levels

	Model no.						
	1	2	3	4	5	6	7
h	0.80	1.00	1.20	1.50	1.80	2.00	2.50
θ_0, deg	10.00	15.00	20.00	25.00	30.00	——	——
ϕ, deg	80.00	90.00	100.00	110.00	120.00	135.00	——

E. Optimization Results

The weight factor β is set to be 0.5, and the `ga` function embedded in MATLAB [22] is employed to solve the optimization problem. The maximum generation is set to be 1000, and the genetic algorithm is terminated when the tolerance between the current objective function and the previous objective function is smaller than 1.0×10^{-8}. The optimization history is presented in Fig. 8. The process is also terminated when the generation reaches 200. The optimum time-averaged thrust coefficient and propulsive efficiency are 1.10 and 0.4731, and the optimum design point is $h = 1.3265$, $\theta_0 = 30.0$, and $\phi = 97.6624$. It should be mentioned that this optimum is similar to Tuncer and Kaya's [7] optimum with $\beta = 0.5$. Similar instantaneous particle traces are shown in [7].

F. Three-Dimensional CFD Analysis

The grid near the 3-D wing is illustrated in Fig. 9, and this 3-D hybrid grid is validated using a 3-D wing with pure plunging motion under the conditions of $k = 3.64$, $h = 0.175$, $u = 0.3$ m/s, $c = 0.1$ m, semispan $b = 0.3$ m, and $Re = 3.0 \times 10^4$. The results are compared with Heathcote et al.'s [14] experimental results and Tang et al.'s [29] computational results, illustrated in Fig. 10. Both of the present results and Tang et al.'s results have a little derivation from the experimental results. However, the present results match well with the previous computational results.

In the case of 2-D computations, the wing tip vortices and the spanwise flows are ignored compared with the 3-D simulations. However, we still can expect that the 2-D result is an acceptable approximation of the 3-D result [30]. The flight condition of the path optimization ($k = 1$, $u = 3.0$ m/s, $c = 0.05$ m and $Re = 1.0 \times 10^4$), wing with AR = 6 and the optimum kinematic parameters are used in the 3-D CFD analysis. The time-averaged thrust coefficient and the propulsive efficiency are shown in Table 3. It is observed that C_T and η obtained by the kriging model and FLUENT at the optimum are very similar (the relative error is less than 5.5%). This validates the kriging model again. The optimum of the 2-D problem is assumed to be the optimum kinematic parameters for the 3-D wing, even though they have a little derivation in the time-averaged thrust coefficient, up to 13.24%. Topology optimization in the next sections is carried out based on this optimum.

Table 2 Validation of the kriging models

				C_D			η		
No.	h	θ_0, deg	ϕ, deg	sModel	FLUENT	Error, %	sModel	FLUENT	Error, %
1	1.60	23.50	103.40	−1.399019	−1.449604	3.50	0.297454	0.296856	0.20
2	1.36	29.60	97.80	−1.159442	−1.138866	1.80	0.451900	0.476958	5.30
3	1.73	23.80	100.70	−1.554946	−1.591267	2.30	0.280245	0.277590	1.00
4	1.52	26.90	87.20	−1.201629	−1.218762	1.40	0.341126	0.355931	4.20
5	1.55	28.60	94.90	−1.423153	−1.468366	3.10	0.374416	0.390918	4.20

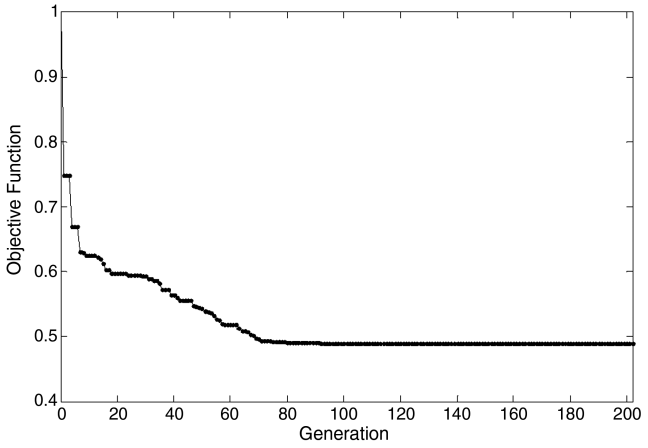

Fig. 8 Convergent history of the genetic algorithm.

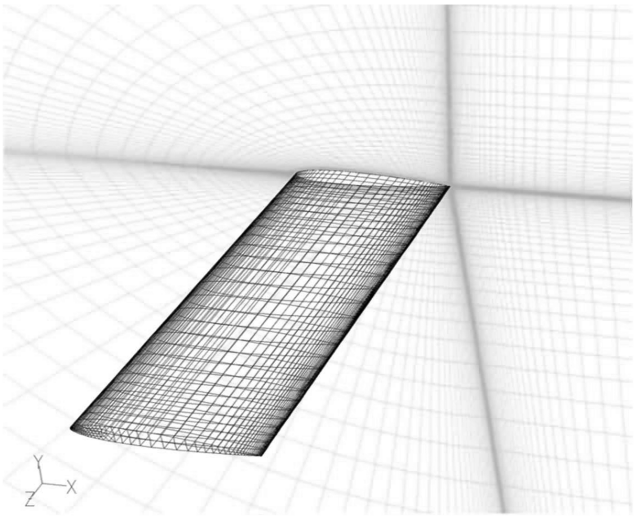

Fig. 9 A structured grid very close to the wing.

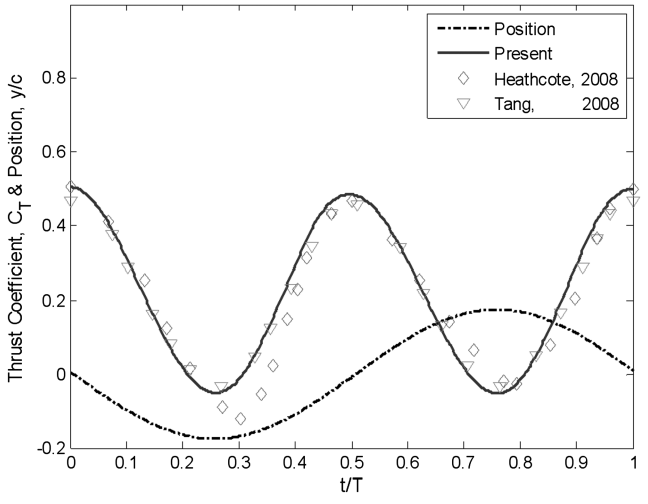

Fig. 10 Validation for a wing with pure plunging motion.

IV. Topology Optimization

The unsteady aerodynamics analysis is performed using the results of path optimization and the dynamic pressures of the surface are obtained. The pressures are applied to the finite element model of the wing for topology optimization. Topology optimization is used to find the optimal layout of a structure within a specified region. In general, the objective function to be minimized in topology optimization is the compliance with an equality constraint upon the volume fraction. Therefore, topology optimization is performed using the results of path optimization in order to reduce the weight and maximize stiffness to find the distribution of reinforcement.

A. Finite Element Model of the Flapping Wing

The surface pressures are obtained by using the optimum values of path optimization. First, the finite element model is generated based on the grid scheme of the unsteady aerodynamics analysis. However, the finite element model is not suitable for structural analysis, because the aspect ratio of the elements is too high. Therefore, the grid is changed for structural analysis and Fig. 11 illustrates the finite element models. All the element pressures of Fig. 11a are obtained from unsteady aerodynamics analysis. The pressures are mapped to the finite element model for structural analysis using a zeroth-order interpolation, as illustrated in Fig. 11b.

Figure 12 presents the finite element model of the wing for topology optimization. The geometry of the wing is the same as the model for 3-D CFD analysis. To maintain the consistency of the model, a 2-D airfoil shape has been extended to the 3-D flapping wing. In the flapping wing, the center point of the leading edge is attached to the frame, as illustrated in Fig. 1. The boundary condition is imposed on the 13 nodes of the center and all the degrees of freedom in the six directions are fixed. The finite element model is composed of two shell element layers with a hollow space in the core, as illustrated in Fig. 13. In Fig. 13, the finite element model is divided into the design domain and the nondesign domain. The inner and outer shell elements of the leading-edge portion are assigned to the nondesign domain, while both ends of the wing are also assigned to the nondesign domain. The number of finite elements is 264 in the nondesign domain.

The design domain is the inner layer of the shell elements and one layer is composed of 3,200 shell elements. Common nodes are used for the outer and inner shell elements. The Young's modulus of the design domain (carbon) is 170.3 GPa, Poisson's ratio is 0.3, and the material density is 2001.2 kg/m^3. Young's modulus of the nondesign domain (mylar) is 3.28 GPa, Poisson's ratio is 0.4, and the material density is 1400.6 kg/m^3. The thickness of the design domain is 1.0 mm and the thickness of the nondesign domain is 0.1 mm. The pressures are always applied on the nondesign domain and the nondesign domain is supported by the design domain. Therefore, the topology of the reinforcement (carbon) is changed during the topology optimization process except for the nondesign domain.

To perform dynamic topology optimization, the surface pressures are calculated at every time step of dynamic analysis and the pressures are applied to the finite element model. The maximum displacement occurs at the wing tip of the trailing edge, and its value is about 0.007 mm in the model of the two layers (carbon and mylar). The loading condition used in 3-D topology optimization is sufficiently representative, because the wing deformation is not too large.

B. General Formulation of Static Topology Optimization

Topology optimization determines the state of material distribution in the structural domain. The intermediate variable is used for a design variable in the density method and has a value from 0 to 1. The design variable determines the existence of the materials. An element does not exist when the value of the design variable is zero and exists when the value of the design variable is 1 [31]. The objective function is the average compliance and the design variables are the intermediate density variables. The topology optimization formulation using linear static response optimization is as follows:

Find

$$b_i \quad i = 1, \ldots, \mathrm{NE}$$

Table 3 Comparison between 2-D and 3-D results

				C_T		η	
Case	h	θ_0	ϕ	Kriging	FLUENT	Kriging	FLUENT
2-D	1.3265	30.0000	97.6624	1.1000	1.0705	0.4731	0.5001
3-D	1.3265	30.0000	97.6624	——	0.9453	——	0.4992

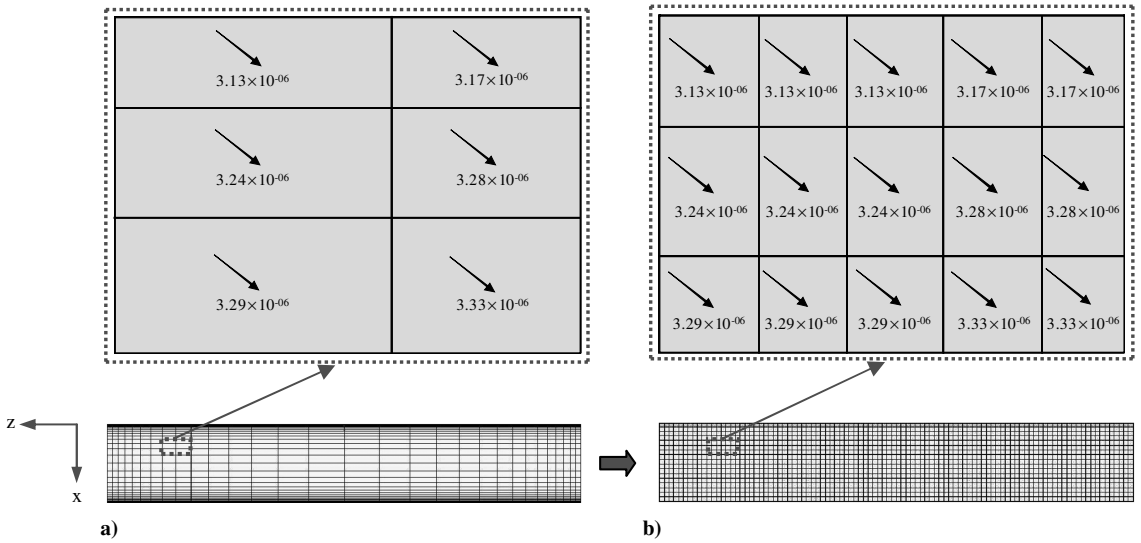

Fig. 11 Application of the pressures of the finite element model: a) unsteady aerodynamic analysis model and b) structural analysis model.

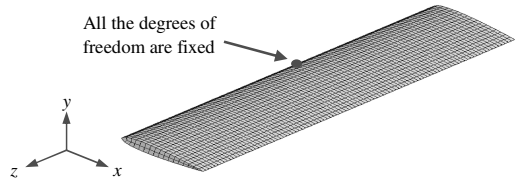

Fig. 12 Finite element model of the wing for topology optimization.

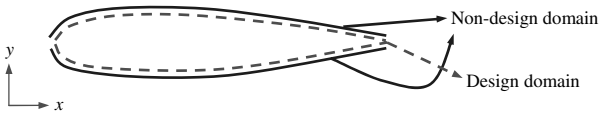

Fig. 13 Design and nondesign domain for topology optimization.

Minimize

$$\mathbf{f}^T\mathbf{z} \tag{15}$$

Subject to

$$\mathbf{K}(\mathbf{b})\mathbf{z} - \mathbf{f} = 0 \qquad \sum_{i=1}^{\mathrm{NE}} v_i b_i \le V$$

$$0 < b_{i,\min} \le b_i \le b_{i,\max} \le 1$$

where b_i is a value for the ith artificial density function as design variables, v_i is the volume of each element, V is the given limit volume of the design domain, $\mathbf{K}(\mathbf{b})$ is the stiffness matrix of the finite element method, $\mathbf{z}$ is the displacement vector, $\mathbf{f}$ is the external force vector, and NE is the total number of design variables. The lower bound of the design variables is $b_{\min}$ and has a very small value close to 0. The upper bound of the design variables is $b_{\max}$ and generally has 1. The strain energy can be used for the objective function instead of the compliance in linear static topology optimization, because compliance is twice the strain energy.

The design variables in topology optimization do not directly correspond to the existence of the material. Therefore, the update method for the material property is used to use the results of the previous iteration in the next iteration. The update rule of the material property for each element is as follows [31]:

$$E_i = (b_i^{(k)})^p E_i^0; \qquad i = 1, \ldots, \mathrm{NE} \tag{16}$$

$$\rho_i = (b_i^{(k)})^q \rho_i^0 \tag{17}$$

where E_i is Young's modulus of the ith element and it represents the stiffness of an isotropic elastic material. ρ_i is the density of the material of the ith element, $b_i^{(k)}$ is a design variable of the ith element at the kth iteration and NE is the number of design variables, which is the number of finite elements in the design area. The value of E^0 means the initial Young's modulus and the value of ρ^0 means the initial density of the material. In general, the value of p is 2 or 3 and the value of q is 1 [24].

C. Formulation of Dynamic Topology Optimization

All the forces in the real world act dynamically on structures and the surface pressures of the wing change in the time during the flapping motion. Thus, design and analysis should be performed based on the dynamic loads. Dynamic topology optimization is performed to find the distribution of reinforcement on the flapping wing.

In dynamic topology optimization, some researchers claimed that the summation of the strain energy during the entire time is minimized [25,32]. Dynamic topology optimization is carried out for the stiffest structure with a specific mass in the time domain. Figure 14 presents examples of the strain energy between the initial model and the optimized model. The initial model has a 100% mass of the structure and the optimized model has a specific mass according to the constraint on the mass fraction. Thus, the strain energy of the optimized model is larger than that of the initial model under the same dynamic load.

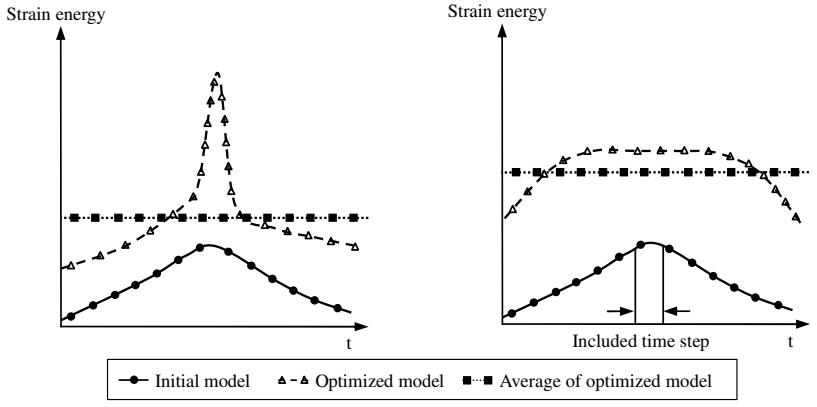

Fig. 14 Strain energy: a) minimization of summations and b) minimization of the peaks.

Figure 14a shows the minimization of strain energy summation during the entire time and Fig. 14b shows the minimization of the peak values of the strain energy. In the optimized model, the strain energy of Fig. 14a can be increased rapidly at a particular time, while the average strain energy of Fig. 14a is smaller than that of Fig. 14b. It means that the deformation of the structure can be very large at a particular time. In Fig. 14b, the average of the strain energy is larger, while the peak is smaller. This means that the deformation of the case in Fig. 14b is more uniform in the time domain. Since a large deformation for even a short time is dangerous to the flapping motion, the peaks of the strain energy should be minimized in dynamic topology optimization. The peaks of the strain energy are found by dynamic analysis. As the design proceeds, the peaks of the current iteration may not be the peaks in the next iteration. Thus, the strain energies for a few time steps near the peaks are minimized, as illustrated in Fig. 14b. In other words, the summation of the strain energy during the included steps is minimized to obtain the topology of the structure.

A dynamic optimization method has been developed for size and shape optimizations based on ESLSO. ESLSO can accommodate dynamic characteristics without complex differential equations. The efficiency of ESLSO has been verified by various researchers [18,33–37]. As mentioned earlier, ESLSO is modified for dynamic topology optimization of the flapping wing. Equivalent static loads (ESLs) are made to generate the same response field as that from dynamic pressures at each time step of unsteady aerodynamics analysis. At the time steps near the peaks of the strain energy, ESLs are calculated and used as the external pressures in static topology optimization.

Dynamic topology optimization using ESLs is formulated as follows:

Find

$$b_i \quad i = 0, \ldots, \mathrm{NE}$$

Minimize

$$S_p \tag{18}$$

Subject to

$$\mathbf{M}(\mathbf{b})\ddot{\mathbf{z}}(t) + \mathbf{C}(\mathbf{b})\dot{\mathbf{z}}(t) + \mathbf{K}(\mathbf{b})\mathbf{z}(t) = \mathbf{f}(t) \quad t = 0, \ldots, l$$

$$\text{mass} \le \text{mass}_{\text{initial}} \times \alpha \qquad 0.0 < b_{i\min} \le b_i \le 1.0$$

The design variable b_i is the design variable of the ith element in the design domain. The objective function, which is S_p, is the summation of the strain energy at the time steps near the peaks of the strain energy. $\mathbf{M}(\mathbf{b})$ is the mass matrix, $\mathbf{C}(\mathbf{b})$ is the damping matrix, $\mathbf{K}(\mathbf{b})$ is the stiffness matrix, $\mathbf{f}(t)$ is the external dynamic force vector, $\mathbf{z}(t)$ is the dynamic displacement vector, t is the time and l is the number of time steps. α is the mass fraction given by the user. The constraint is that the mass of the structure should be less than $\alpha\%$ of the mass of the initial structure. The mass of the initial structure is the mass of the structure when all the design variables have 1.0.

D. ESLSO for Topology Optimization

ESLSO is a method for dynamic response optimization of structures. The static loads are made to generate the same displacement field as dynamic loads at each time steps and the loads are called equivalent static loads. The ESLs are used to static response optimization, because the loads remove the time-dependent constraint conditions. Calculated ESLs at each time step are used as multiple loading conditions in topology optimization. The process of calculating ESLs is explained. The governing equation of dynamic analysis is

$$\mathbf{M}(\mathbf{b})\ddot{\mathbf{z}}(t) + \mathbf{C}(\mathbf{b})\dot{\mathbf{z}}(t) + \mathbf{K}(\mathbf{b})\mathbf{z}(t) = \mathbf{f}(t) \quad t = 0, \ldots, l \tag{19}$$

where $\mathbf{M}(\mathbf{b})$ is the mass matrix, $\mathbf{C}(\mathbf{b})$ is the damping matrix, $\mathbf{K}(\mathbf{b})$ is the stiffness matrix, $\mathbf{z}(t)$ is the dynamic displacement vector, t is the time and l is the number of time steps. The ESLs are calculated as

$$\mathbf{f}_{\text{eq}}(s) = \mathbf{K}(\mathbf{b})\mathbf{z}(s) \quad s = 0, \ldots, l \tag{20}$$

where $\mathbf{f}_{\text{eq}}(s)$ is the ESLs vector, $\mathbf{K}(\mathbf{b})$ is the stiffness matrix, and s is the loading case, which is equivalent to t in Eq. (19). The number of ESLs is the same as that of the time steps.

ESLSO was originally developed for size/shape optimization. A preliminary study on topology optimization using ESLs was performed for a small-scale standard problem [25]. As mentioned earlier, since the summation of the strain energy in the entire time domain was minimized in [25], the optimum topology was not practical. In this research, the method is modified to minimize the peaks and applied to the design of a flapping wing. The process of topology optimization using ESLSO is as follows:

Step 1) Set cycle number $k = 0$, and the design variables $\mathbf{b}^{(k)} = \mathbf{b}^{(0)}$.

Step 2) Perform dynamic analysis with $\mathbf{b}^{(k)}$.

Step 3) Calculate ESLs in the time domain by using Eq. (20).

Step 4) Perform static topology optimization as follows:

Find

$$\mathbf{b}^{(k+1)} \in R^n$$

Minimize

$$f(\mathbf{b}^{(k+1)}, \mathbf{z}) \tag{21}$$

Subject to

$$\mathbf{K}(\mathbf{b}^{(k+1)})\mathbf{z}(s) = \mathbf{f}_{\text{eq}}^{(k)}(s) \quad s = 1, \ldots, l$$

$$g_j(\mathbf{b}^{(k+1)}, \mathbf{z}) \le 0 \quad j = 1, \ldots, m$$

$$0.0 < b_{\min} \le b_i^{(k+1)} \le 1.0 \quad i = 1, \ldots, n$$

where the design variables are the density of each element and the objective function is the summation of strain energy at the time steps near the peaks of the strain energy.

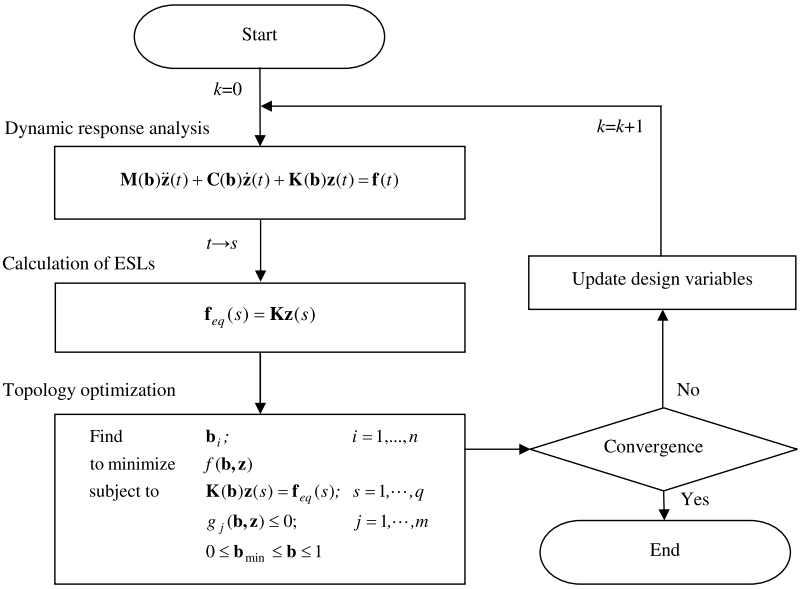

Fig. 15 Process of topology optimization using ESLSO.

Step 5) When $k = 0$, go to step 6. Otherwise, check the convergence. If the convergence criterion is satisfied, the optimization process terminates. If the convergence criterion is not satisfied, go to step 6.

Step 6) Update the design, set $k = k + 1$, and go to step 2.

The process is repeated until the convergence criterion is satisfied. The repetition process is called a cycle. The difference of dynamic and static responses is decreased as the repetition proceeds. The overall process is illustrated in Fig. 15.

1. Convergence Criterion

The convergence criterion for size and shape optimizations using ESLSO is defined as

$$\sum_{i=1}^{n} |b_i^{(k)} - b_i^{(k-1)}| \le \varepsilon_1 \tag{22}$$

where ε_1 is a user-defined small number. After static topology optimization, if the change of design variables from the previous cycle is small, the process terminates. However, it is difficult to satisfy the condition of Eq. (22) in topology optimization, because some design variables have repeated values of 0 and 1. Therefore, a new convergence criterion for topology optimization is defined as

$$\text{countif}\,(|b_i^{(k)} - b_i^{(k-1)}| \ge \varepsilon_1) \le n \times \varepsilon_2 \quad i = 1, \ldots, n \tag{23}$$

where ε_2 is another user-defined small number. In Eq. (23), the number of design variables that change more than ε_1 are counted first. If the counted number is less than the certain value $n \times \varepsilon_2$, then the process terminates. The convergence criterion in Eq. (23) is used in step 5.

2. Method for Design Update

In general static topology optimization, the update method of the material property is in Eqs. (16) and (17) and this update method is made for static topology optimization. The update method between the cycles is newly defined for dynamic topology optimization. The optimum design variables from static topology optimization have the values in the continuous space from 0.0 to 1.0. After static topology optimization is finished, the elements less than a user-defined small number ε_3 are removed and the design variables for the elements larger than ε_3 remain. It is noted that ε_3 should be fairly small, because the results with a large ε_3 deteriorate the connectivity of the elements. Even a small ε_3 removes the elements quite a lot. The density of an element is changed so that a removed element has 0.0 and the remaining element has 1.0. The new density is updated and dynamic analysis is performed with the new densities in the next cycle.

E. Results of Topology Optimization

As mentioned earlier, dynamic topology optimization is performed to find the reinforcement of the flapping wing. The dynamic pressure from the 3-D CFD analysis is imposed on the flapping wing as the external loads. The number of the time steps near a peak is set by five and ESLSO is used for dynamic topology optimization. Since the actual target model of Fig. 1 is close to a flat plate structure, the reinforcement distribution is assumed to be identical in the upper and lower layers. The results of dynamic topology optimization are illustrated in Fig. 16.

Figure 16a is the result of dynamic topology optimization of the flapping wing when the mass fraction is 10%, ε_1 is 0.3, ε_2 is 0.2, and ε_3 is 0.00001. Figure 16b) is the results of dynamic topology optimization when the mass fraction is 5%, ε_1 is 0.1, ε_2 is 0.1 ε_3 is 0.00001. The remaining elements show the distribution of the reinforcement of the wing. The elements of the leading-edge portion remain by selecting the nondesign domain. The final optimization results in Fig. 16 only show the Z–X plane view, because the optimization results of the upper and lower layers have the same topology. The results mean reinforcement distribution of the stiffest structure with specific mass fractions.

The structure of the flapping wing should have some flexibility and certain rigidity and a small amount of rigidity guarantees flexibility [14,38,39]. However, how flexible or rigid the wing should be is not fully studied yet for each flapping wing. This research only shows that the results of dynamic topology optimization can keep a certain rigidity with a specific mass. If the target rigidity is identified,

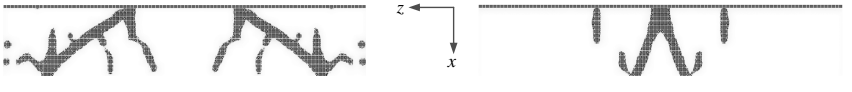

a) **b)**

Fig. 16 Results of dynamic topology optimization: a) mass fraction 0.1 and b) mass fraction 0.05.

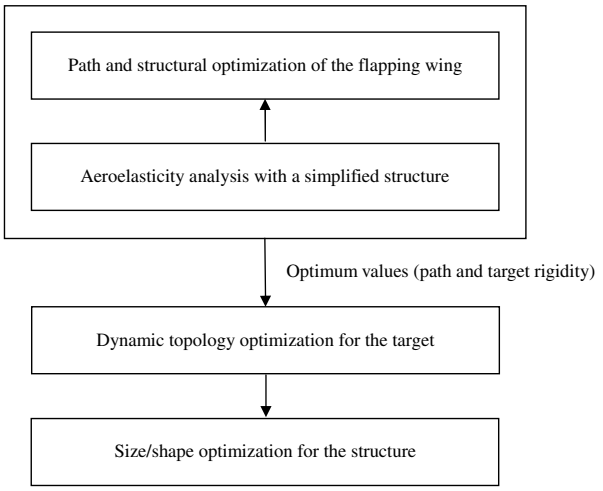

Fig. 17 Scenario for future direction.

topology optimization can be performed to meet the target rigidity. This aspect will be explained in the next section.

V. Future Direction for the Design of the Flapping Wing

This study shows the possibility of optimizing the flapping-wing system. However, all the involved disciplines are separately considered. Therefore, the optimum solution is obtained in a local sense. In the future, they should be considered simultaneously. A direction of the future study is illustrated in Fig. 17. To include the stiffness of the structure, path optimization should be simultaneously performed with structural optimization and aeroelasticity analysis is required in this process. Besides, the research should consider anisotropic flexibility, the study of the relationship between aerodynamic characteristics and the deformation of the chord and spanwise. Through this study, the appropriate anisotropic material properties (e.g., Young's modulus, Poisson's ratio) can be determined for structural optimization.

A high-fidelity structural model may cost too much in this optimization process. So a low fidelity (simplified) structural model can be exploited, and the approximation method of this research can be used in this process. Path optimization is performed using the simplified structural model based on the proposed optimization process and aeroelasticity analysis will be used to consider the inertial effect of the flexible wing. The flapping kinematics can be defined from the results of path optimization. The appropriate flexibility can be identified, because the flapping kinematics of the flexible wing is determined. Then the target for rigidity is automatically evaluated and dynamic topology optimization is performed to meet the target based on various mass fractions. In the results of dynamic topology optimization, the reinforcement distribution of minimum mass can be selected. The reinforcement distribution to enhance the aerodynamic characteristics, which satisfy some rigidity, and minimum mass can be found.

As mentioned earlier, quantitative research on the amount of rigidity is required and the problem can be solved in the process. The external loads are made by the method of this research. For a final detailed design, size/shape optimization is performed to meet the target while various design conditions are satisfied. Eventually, multidisciplinary design optimization will be employed, because the involved disciplines are coupled.

VI. Conclusions

Rigidity and the mass of the flapping wing are important factors in terms of aerodynamic performance. In this research, a work flow for the design of the flapping wing is defined. A flapping system is optimized and path optimization is conducted to enhance the performances such as thrust and propulsive efficiency. The kriging method is employed for optimization and CFD analysis for a 2-D airfoil is used for the optimization process. The results of CFD analysis are verified by using some references. A genetic algorithm is used for the multi-objective function problem of the path optimization. The flapping path is determined and the determined path is used for dynamic topology optimization of the wing structure. The peaks of the strain energy are minimized to find the stiffest structure. The external loads are calculated from a 3-D CFD airfoil analysis. Reinforcement within the wing is determined to have certain rigidity with a specific mass. Since the external loads are dynamically imposed in the time domain, a dynamic topology optimization method is newly developed by using the equivalent static loads. The reinforcement distributions of the flapping wing are found when the mass fraction is 5 and 10%.

Consequently, the following conclusions are made:

1) The path optimization is carried out by the kriging method and a genetic algorithm.

2) The newly developed dynamic topology optimization method can be applied to dynamic response optimization of a flapping-wing system.

3) The best reinforcement distribution of the flapping-wing structure can be found for excellent aerodynamic and structural characteristics by the proposed work flow.

Since the research is in the early stage, future direction for the research is proposed.

Acknowledgments

This research was supported by Asian Office of Aerospace Research and Development (AOARD-05-4015) and the World Class University program through the Korea Science and Engineering Foundation funded by the Ministry of Education, Science and Technology (no. R32-2008-000-10022-0). This research was also supported by Basic Science Research Program through the National Research Foundation of Korea funded by the Ministry of Education, Science and Technology (2011-0025859). The authors are thankful to MiSun Park for her English correction of the manuscript.

References

[1] McMichael, J. M., and Francis, M. S., "Micro Air Vehicles—Toward a New Dimension in Flight," Defense Advanced Research Projects Agency, Arlington, VA, 1997.

[2] Garrick, I. E., "Propulsion of a Flapping and Oscillating Airfoil," NACA Rept. 567, 1937.

[3] Young, J., Walker, S. M., Bomphrey, R. J., Taylor, G. K., and Thomas, L. R., "Details of Insect Wing Design and Deformation Enhance Aerodynamic Function and Flight Efficiency," *Science*, Vol. 325, No. 5947, 2009, pp. 1549–1552. doi:10.1126/science.1175928

[4] Jones, K. D., and Platzer, M. F., "Bio-Inspired Design of Flapping Wing Micro Air Vehicles—An Engineer's Perspective," AIAA Paper 2006-0037.

[5] Anderson, J. M., Streitlien, K., Barrett, D. S., and Triantafyllou, M. S., "Oscillating Foils of High Propulsive Efficiency," *Journal of Fluid Mechanics*, Vol. 360, 1998, pp. 41–72. doi:10.1017/S0022112097008392

[6] Pesavento, U., and Wang, Z. J., "Flapping Wing Flight Can Save Aerodynamic Power Compared to Steady Flight," *Physical Review Letters*, Vol. 103, 2009, Paper 118102. doi:10.1103/PhysRevLett.103.118102

[7] Tuncer, H. I., and Kaya, M., "Optimization of Flapping Airfoils for Maximum Thrust and Propulsive Efficiency," *AIAA Journal*, Vol. 43, No. 11, 2005, pp. 2329–2336. doi:10.2514/1.816

[8] Kaya, M., and Tuncer, H. I., "Nonsinusoidal Path Optimization of a Flapping Airfoil," *AIAA Journal*, Vol. 45, No. 8, 2007, pp. 2075–2082. doi:10.2514/1.29478

[9] Kaya, M., Tuncer, H. I., Jones, D. K., and Platzer, M., "Optimization of Flapping Motion Parameters for Two Airfoils in a Biplane," *Journal of Aircraft*, Vol. 46, No. 2, 2009, pp. 583–592. doi:10.2514/1.38796

[10] Soueid, H., Guglielmini, L., Airiau C., and Bottaro, A., "Optimization of the Motion of a Flapping Airfoil Using Sensitivity Functions," *Computers and Fluids*, Vol. 38, 2009, pp. 861–874.

doi:10.1016/j.compfluid.2008.09.012
[11] Simpson, T. W., Mauery, T. M., Korte, J. J., and Mistree, F., "Kriging Models for Global Approximation in Simulation-Based Multidisciplinary Design Optimization," *AIAA Journal*, Vol. 39, No. 12, 2001, pp. 2233–2241. doi:10.2514/2.1234
[12] Queipo, N. V., Haftka, R. T., Shyy, W., Goel, T., Vaidyanathan R., and Tucker. P. K., "Surrogate-Based Analysis and Optimization," *Progress in Aerospace Sciences*, Vol. 41, 2005, pp. 1–28. doi:10.1016/j.paerosci.2005.02.001
[13] Miao, J. M., and Ho, M. H., "Effect of Flexure on Aerodynamic Propulsive Efficiency of Flapping Flexible Airfoil," *Journal of Fluids and Structures*, Vol. 22, 2006, pp. 401–419. doi:10.1016/j.jfluidstructs.2005.11.004
[14] Heathcote, S., Wang, Z., and Gursul, I., "Effect of Spanwise Flexibility on Flapping Wing Propulsion," *Journal of Fluids and Structures*, Vol. 24, No. 2, 2008, pp. 183–199. doi:10.1016/j.jfluidstructs.2007.08.003
[15] Stanford, B., and Ifju, P., "Aeroelastic Topology Optimization of Membrane Structures for Micro Air Vehicles," *Structural and Multidisciplinary Optimization*, Vol. 38, No. 3, 2009, pp. 301–316. doi:10.1007/s00158-008-0292-x
[16] Choi, W. S., and Park, G. J., "Transformation of Dynamic Loads into Equivalent Static Loads Based on Modal Analysis," *International Journal for Numerical Methods in Engineering*, Vol. 46, No. 1, 1999, pp. 29–43. doi:10.1002/(SICI)1097-0207(19990910)46:1<29::AID-NME661>3.0.CO;2-D
[17] Kim, Y. I., Park, G. J., Kolonay, R. M., Blair, M., and Canfield, R. A., "Nonlinear Dynamic Response Structural Optimization of a Joined-Wing Using Equivalent Static Loads," *Journal of Aircraft*, Vol. 46, No. 3, 2009, pp. 821–831. doi:10.2514/1.36762
[18] Park, G. J., "Technical Overview of the Equivalent Static Loads Method for Non Linear Static Response Structural Optimization," *Structural and Multidisciplinary Optimization*, Vol. 43, No. 3, 2011, pp. 319–337. doi:10.1007/s00158-010-0530-x
[19] ANSYS FLUENT, User's Guide, Ver. 12.1, ANSYS, Inc., Canonsburg, PA, 2009.
[20] MD R3 Nastran, User's Guide, MSC Software Corp., Santa Ana, CA, 2008.
[21] GENESIS, Software Package, Ver. 10.0, Vanderplaats Research and Development, Inc., Colorado Springs, CO, 2008.
[22] MATLAB, Software Package, Ver. 7.9, The MathWorks, Inc., Natick MA, 2009.
[23] Stroustrup, B, *The C++ Programming Language*, Addison Wesley, Reading, MA, 2000.
[24] Bensoe, M. P., and Sigmund, O., *Topology Optimization: Theory, Methods and Application*, Springer, Berlin, 2002.
[25] Jang, H. H., Lee, H. A., and Park, G. J., "Preliminary Study on Linear Dynamic Response Topology Optimization Using Equivalent Static Loads," *Transactions of the Korean Society of Mechanical Engineers. A.*, Vol. 33, No. 12, 2009, pp. 1401–1409. doi:10.3795/KSME-A.2009.33.12.1401 (in Korean).
[26] GAMBIT, User's Guide, Ver. 2.3.16, Fluent, Inc., Canonsburg, PA, 2006.
[27] Kinsey, T., and Dumas, G., "Parametric Study of an Oscillating Airfoil in a Power-Extraction Regime," *AIAA Journal*, Vol. 46, No. 6, 2008, pp. 1318–1330. doi:10.2514/1.26253
[28] Tuncer, I. H., and Kaya, M., "Thrust Generation Caused by Flapping Airfoils in a Biplane Configuration," *Journal of Aircraft*, Vol. 40, No. 3, 2003, pp. 509–515. doi:10.2514/2.3124
[29] Tang, J., Chimakurthi, S., Palacios, R., Cesnik C., and Shyy, W., "Computational Fluid-Structure Interaction of a Deformable Flapping Wing for Micro Air Vehicle Applications," AIAA Paper 2008-0615.
[30] Wang, Z. J., Birch, J. M., and Dickinson, M. H., "Unsteady Forces and Flows in Low Reynolds Number Hovering Flight: Two-Dimensional Computations vs Robotic Wing Experiments," *Journal of Experimental Biology*, Vol. 207, 2004, pp. 449–460. doi:10.1242/jeb.00739
[31] Park, G. J., *Analytic Methods for Design Practice*, Springer, Berlin, 2007.
[32] Min, S., Kikuchi, N., Park, Y. C., Kim, S., and Chang, S., "Optimal Topology Design of Structures Under Dynamic Loads," *Structural and Multidisciplinary Optimization*, Vol. 17, Nos. 2–3, 1999, pp. 208–218.
[33] Park, G. J., and Kang, B. S., "Validation of a Structural Optimization Algorithm Transforming Dynamic Loads into Equivalent Static Loads," *Journal of Optimization Theory and Applications*, Vol. 118, No. 1, 2003, pp. 191–200. doi:10.1023/A:1024799727258
[34] Park, K. J., Lee, J. N., and Park, G. J., "Shape Optimization Under Static Loads Transformed from Dynamic Loads," *Fifth World Congress of Structural and Multidisciplinary Optimization*, Lido di Jesolo, Italy, 2003, pp. 219–220.
[35] Shin, M. K., Park, K. J., and Park, G. J., "Optimization of Structures with Nonlinear Behavior using Equivalent Loads," *Computer Methods in Applied Mechanics and Engineering*, Vol. 196, No. 4–6, 2007, pp. 1154–1167. doi:10.1016/j.cma.2006.09.001
[36] Kang, B. S., Park, G. J., and Arora, J. S., "Optimization of Flexible Multibody Dynamic System Using the Equivalent Static Load Method," *AIAA Journal*, Vol. 43, No. 4, 2005, pp. 846–852. doi:10.2514/1.4294
[37] Kim, Y. I., and Park, G. J., "Nonlinear Dynamic Response Structural Optimization Using Equivalent Static Loads," *Computer Methods in Applied Mechanics and Engineering*, Vol. 199, No. 9–12, 2010, pp. 660–676. doi:10.1016/j.cma.2009.10.014
[38] Combes, S. A., and Daniel, T. L., "Flexural Stiffness in Insect Wings I: Scaling and the Influence of Wing Venation," *Journal of Experimental Biology*, Vol. 206, No. 17, 2003, pp. 2979–2987. doi:10.1242/jeb.00523
[39] Kim, D. K., and Han, J. H., "Optimal Design of a Flexible Flapping Wing Using Fluid-Structure Interaction Analysis," *8th International Conference on Motion and Vibration Control*, Technical Univ. of Munich, Munich, Sept. 15–18 2008.

A. Messac
Associate Editor